

Calculation of the wall-pressure field in a turbulent channel flow

R. A. Handler, R. J. Hansen, and L. Sakell
Naval Research Laboratory, Washington, D.C. 20375

S. A. Orszag and E. Bullister
Massachusetts Institute of Technology, Cambridge, Massachusetts 20139

(Received 28 September 1983; accepted 17 November 1983)

The wall-pressure field in a turbulent channel flow has been obtained from a numerical solution of the Navier–Stokes equations. The root mean square pressure normalized with respect to the wall shear stress, as well as the convection velocity of the field, are in good agreement with experiment. Certain limitations of the calculation, associated with its finite spatial resolution, are discussed.

I. INTRODUCTION

The spectral properties of the turbulent pressure field at the surface of a structure are needed for the calculation of its vibration and the estimation of the radiated acoustic field. In addition, its spatial and temporal properties give insight into the eddy, or “wavelike” structure of the turbulent velocity field. Here we present the results of a calculation of the wall pressure field of a turbulent channel flow directly from the numerical solution of the Navier–Stokes equations, in which no closure assumptions are employed.

Previous theoretical estimates of the spectral properties of the wall-pressure field in wall-bounded turbulent shear flows have relied on empirical information about the velocity field. Kraichnan¹ concludes that the turbulence–mean-shear interaction is the dominant source of the wall-pressure fluctuations. He estimates on this basis that $(\overline{p^2})^{1/2} = 6 \tau_w$, where $(\overline{p^2})^{1/2}$ is the root mean square wall pressure at a point and τ_w is the mean wall shear stress. Empirical input is used by Panton and Linebarger² to obtain wavenumber spectra in good agreement with experiment. Using limited empirical information, Landahl’s³ waveguide model gives two point cross-spectral results which agree well with experiment.

In contrast to the previous work, we demonstrate that the most significant statistical properties of the wall-pressure field can be obtained from the governing equations of fluid dynamics. We rely on the methods given in Ref. 4. In that work, the solution to a fully developed channel flow is obtained. The Reynolds number (R) is 5000 based on the channel half-width h and U , the laminar centerline velocity. Unless otherwise stated all other variables are scaled on U and h . A pseudospectral computational procedure, in which all spatial derivatives are evaluated in the spectral domain and temporal derivatives in the physical domain, is used. Full use is made of optimized fast Fourier transforms (FFT’s) to go between physical and spectral domains and to evaluate derivatives in terms of the recursion properties of the Chebyshev expansion functions employed. Using this procedure, mean velocity profiles, Reynolds stresses, and turbulent intensities are found to be in good agreement with experiment. This calculation differs from that of Kim and Moin⁵ who employed a closure assumption for the smallest scales of turbulent motion and obtained results for some-

what higher Reynolds’ numbers (13 000 based on channel half-width). The present results are obtained using 32 spectral functions in each spatial direction [i.e., $(32)^3$ modes] in contrast to the $(64)^3$ calculation of Ref. 4.

The Navier–Stokes equations are solved in rotation form

$$\frac{\partial \mathbf{v}}{\partial t} = \mathbf{v} \times (\nabla \times \mathbf{v}) - \nabla \left(p + \frac{1}{2} v^2 \right) + \frac{1}{R} \nabla^2 \mathbf{v} + \frac{2}{R} \hat{x}, \quad (1)$$

$$\nabla \cdot \mathbf{v} = 0, \quad (2)$$

where \mathbf{v} is the velocity and \hat{x} is the unit vector in the flow direction. It follows that the pressure field p is given by solving the Poisson equation

$$\nabla^2 (p + \frac{1}{2} v^2) = \nabla \cdot [\mathbf{v} \times (\nabla \times \mathbf{v})], \quad (3)$$

$$\frac{\partial p}{\partial z} = 0 \quad (z = \pm 1), \quad (4)$$

where the channel walls are at $z = \pm 1$.

II. DATA ANALYSIS

The wall-pressure field, $p(x, y, t)$, where x and y are the streamwise and spanwise coordinates, respectively, and t is the time, is computed at each of $32 \times 32 = 1024$ spatial locations. The spatial separation between points was 0.162 (i.e., about 16% of the half-width), and the time interval between each spatial computation was 0.02. It has been shown in Ref. 4 that the flow becomes quasistationary for $t \gtrsim 40$. During this interval, R^* , the Reynolds number based on friction velocity u_* , where $u_* = (\tau_w/\rho)^{1/2}$, and ρ is the density, varies between about 190 and 200. Therefore, the pressure–time histories generated for $40 \leq t \leq 60$ are chosen as best representing a stationary random process and are used in all spectral computations.

The viewpoint taken here is that the numerically generated wall-pressure data should be analyzed in the same manner as one would process experimental time domain data. In contrast to an experiment, however, where sufficient time domain data exists to give adequate frequency resolution and minimal random errors, the present run is limited to 1000 time domain points per spatial location. In an experiment, one may, for example, form the cross spectrum of the fluctuating pressure at some streamwise location x_0 and spanwise location y_0 with the pressure at $x_0 + \Delta x$ and y_0 . The random error is reduced in this case by ensemble averaging.

ing over many statistically independent estimates of the spectrum. In the present case, however, because of the limited time domain data and the need to resolve low-frequency information (i.e., $fh/U \lesssim 1.0$), it is necessary to ensemble average over the spanwise coordinate. More specifically, an estimate of the cross spectrum ϕ between data at streamwise locations x_0 and $x_0 + \Delta x$, with the spanwise position fixed at y_0 , is given by⁶

$$\phi(f, \Delta x; x_0) = (2/T)E [P_k^*(x_0, y_0, f)P_k(x_0 + \Delta x, y_0, f)], \quad (5)$$

in which f is the frequency, P is the Fourier transform of p , T is the sampling time interval, and E denotes the expected value operation over the index k . In this case, statistically independent estimates of P_k are obtained by using nonoverlapping time segments of duration T . In contrast, in the present work we obtain the spectral estimate as follows:

$$\phi(f, \Delta x; x_0) = (2/T)E [P_k^*(x_0, y_k, f)P_k(x_0 + \Delta x, y_k, f)], \quad (6)$$

in which the expected value is taken over the y_k 's. In this case, each Fourier transform P_k is taken over the same time interval of duration T . Obtaining spectral estimates in this manner depends on the spatial homogeneity as well as the temporal stationarity of the field. In addition, the spectral estimates ϕ_k will be statistically independent when the separation Δy is much larger than the spanwise coherence length. As a result, for a fixed number of ensemble averages, the random error associated with the estimate obtained by Eq. (6) will, in general, be greater than that associated with Eq. (5). The spectral estimates are obtained using ten ensemble averages with a FFT length of 1024 (i.e., 24 zeros are added to the 1000 available time domain points) giving a frequency spacing, Δf , of 0.049. A Hanning window is used throughout the analysis. Ensemble averages are obtained using a spanwise spacing, Δy , of 0.162.

III. RESULTS

Typical time domain behavior of the wall-pressure field is shown in Fig. 1 in which $p/\frac{1}{2}\rho U_{cl}^2$, where U_{cl} is the centerline velocity, is plotted against nondimensional time tU_{cl}/h . (The centerline velocity is found to be 0.75 ∓ 0.02 during the run and 0.75 was used in Fig. 1.) The two pressure-time histories are generated at the same spanwise location but with a streamwise separation of 0.162 (i.e., the smallest separation in this simulation). The records are typical of broadband random data in that no distinct periodicities can

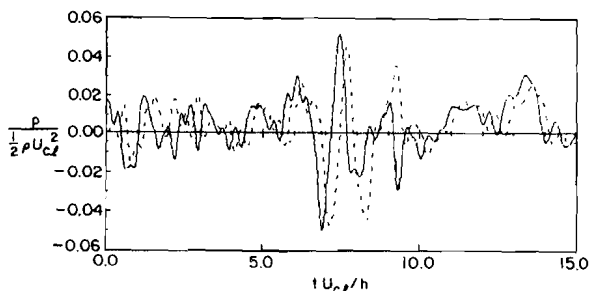


FIG. 1. Typical computed pressure time histories for the same spanwise location and $\Delta x/h = 0.162$.

be observed. At this spatial separation, the field appears to retain a significant degree of coherence and has clearly shifted in the flow direction. These features are qualitatively consistent with the known convective nature of the wall-pressure field. The computed value for $(\overline{p^2})^{1/2}/\tau_w$ is 3.32 ∓ 0.12 , which is in excellent agreement with the experimental results of Blake.⁷

In Fig. 2, the computed spectral density of the pressure field $\phi(f)$ normalized with respect to the wall shear stress, is plotted against the Strouhal number and is compared with both boundary-layer⁷⁻⁹ and pipe flow¹⁰ results. [The spectral density is defined such that $\overline{p^2} = \int_0^\infty \phi(f) df$.] The agreement with experiment is good for $0.4 \lesssim fh/U_{cl} \lesssim 2.0$. At a Strouhal number of about 2.5, we observe a sharp drop in the computed spectral level. We speculate, for reasons given in Sec. IV, that this is due to the finite spatial resolution of the calculation (i.e., the smallest scales of turbulence cannot be resolved). We note that similar behavior is found in experiments in which larger pressure sensors reduce the response at high wavenumbers. As a result, the corresponding spectral density is reduced significantly at high frequencies as shown in Fig. 2 for boundary-layer data in which the ratio d/δ^* , where d is the transducer diameter and δ^* is the displacement thickness, is varied. (We note, however, that the wavenumber filtering produced in the simulation is not mathematically equivalent to the experimentally induced filtering.)

The space-time cross-correlation function, $R(\Delta x, \Delta y, \tau)$, in which τ is a time delay, is given by

$$R(\Delta x, \Delta y, \tau) = \int_0^\infty \phi(\Delta x, \Delta y, f) e^{i2\pi f\tau} df, \quad (7)$$

in which ϕ is given by Eq. (6). In Fig. 3, the function $R(\Delta x, 0, \tau)$ is plotted in nondimensional form. The dominant characteristic of the wall-pressure field, that of a convecting pattern which rapidly loses coherence, is clearly exhibited.

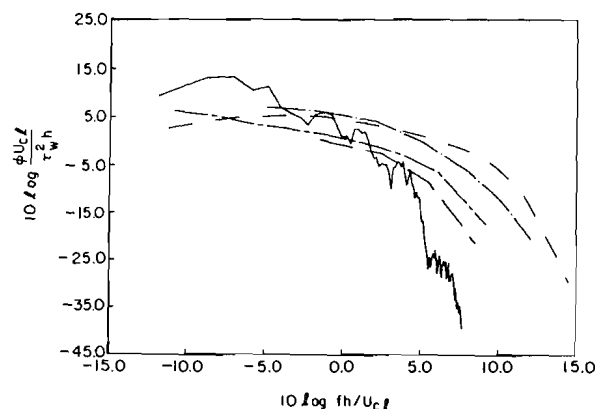


FIG. 2. Comparison of computed and experimental pressure spectral densities: —computed; ---Blake (1970), boundary layer, $d/\delta^* = 0.11$; - · - Willmarth and Woolridge (1962), boundary layer, $d/\delta^* = 0.33$; - - - Corcos (1964), pipe flow; and - - - Scholemer (1966), boundary layer, $d/\delta^* = 0.41$. For boundary layer flows, data is scaled with δ , the boundary layer thickness, and U_∞ . For pipe flow, the data is scaled with r , the pipe radius.

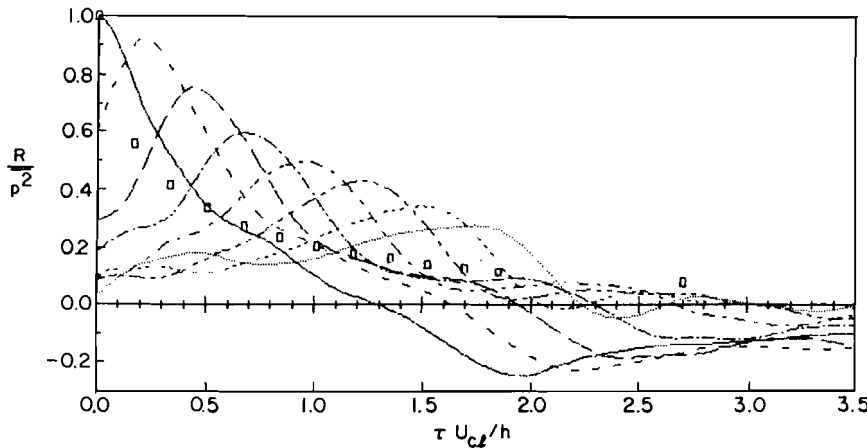


FIG. 3. Computed streamwise space-time cross correlation and comparison with experimental upper bound of Blake (1970), \square . Computed curves are shown in increments of $\Delta x/h = 0.162$.

For comparison, the upper bound of Blake's data is shown. The more rapid decay of the measured field is again due to the limited spatial resolution of the computed results. That is, a lower cutoff frequency in ϕ results [see Eq. (7)] in a slower correlation decay rate. We also note that the shapes of the correlation curves lose symmetry (consistent with experiment), indicating a weakly dispersive behavior. The ratio of the longitudinal integral length scale L_x , where $L_x = \int_0^\infty R(\Delta x, 0, 0) d(\Delta x)$, and the lateral integral length scale L_y , where $L_y = \int_0^\infty R(0, \Delta y, 0) d(\Delta y)$, is about 0.89.

The average broadband convective velocity \bar{U}_c , defined by $\bar{U}_c = \Delta x / \tau_m$, where τ_m is the time delay corresponding to the maximum correlation coefficient for a given Δx , is shown in Fig. 4(a) along with the data of Blake. In contrast to the experimental results, the computed convection velocities do not increase with increasing separation but show a slight decrease before reaching an asymptotic value of about 0.65. This is somewhat smaller than the experimental value. The integral time corresponding to the decay of the field τ_0 , defined by $\tau_0 = \int_0^\infty R(\Delta x, 0, \tau_m) d\tau_m$, can be used to compute the longitudinal correlation length L^* , by $L^* = \tau_0 \bar{U}_c$. The ratio of L^* to L_x is found to be about 2.8. This is somewhat less than the ratio found in pipe flow by Clinch.¹¹

In Fig. 4(b), the phase speed, U_p , given by $U_p = 2\pi f \Delta x / \alpha$, where α is the phase of the cross spectrum, is plotted against Strouhal number. The agreement with the data of Blake is excellent up to $fh/U_{cl} \approx 2.0$. At higher Strouhal numbers, the phase speed becomes large. We speculate on the reasons for this difference in Sec. IV.

IV. DISCUSSION

We estimate from the Nyquist criterion the smallest wavelength that can be resolved in this simulation (λ_{\min}) as $\lambda_{\min} \sim 2\Delta x_{\min}$, where Δx_{\min} is the smallest grid spacing. Therefore, the highest frequency that can be resolved is about $\bar{U}_c / \lambda_{\min}$. Using $\Delta x_{\min}/h = 0.162$ and $\bar{U}_c/U_{cl} \sim 0.65$, we get $f_{\max} h/U_{cl} \approx 2.0$. We observe that this is very close to the "cutoff" frequency exhibited in Fig. 2 and the frequency above which U_p becomes large [see Fig. 4(b)]. In this regard, limited spatial resolution can lead to aliasing which has the effect of artificially increasing the observed phase speeds above f_{\max} . These considerations lead us to believe that spa-

tial resolution limitations can account for some of the differences between our results and experiment. (These observations will be discussed in more detail in a future paper.) We note further that experiments on the wall-pressure field have been performed at Reynolds numbers which are typically one to two orders of magnitude greater than the Reynolds number (5000) used in this simulation. However, as observed by Corcos, the use of τ_w in normalizing the spectral density appears to give data collapse over a wide range of Reynolds

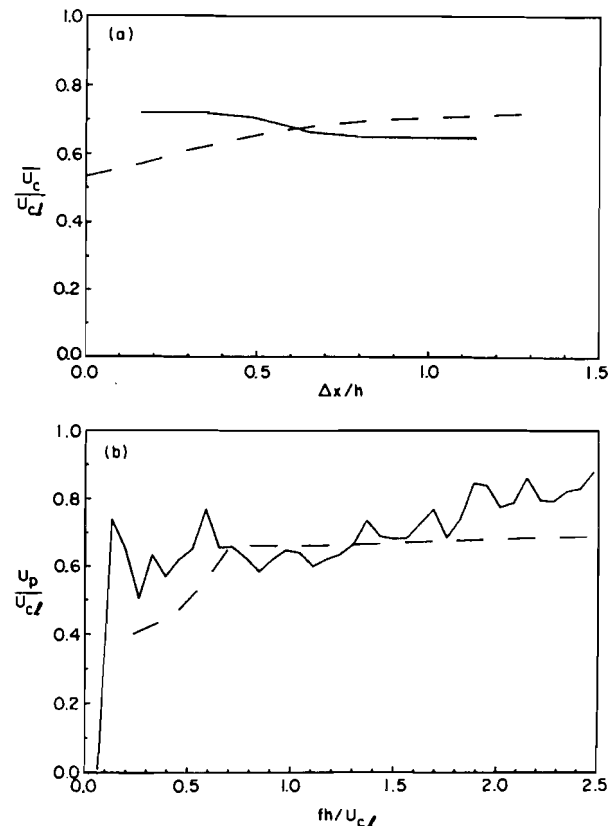


FIG. 4. Comparison of computed and experimental convection velocities. (a) Broadband velocities: —computed; and — —Blake (1970). (b) Narrow-band velocities: —computed, $\Delta x/h = 0.162$; and — —Blake (1970), $\Delta x/h = 0.30$ (δ = boundary layer thickness).

numbers. This is consistent with the excellent agreement between the calculated value for $(\overline{p^2})^{1/2}/\tau_w$ and the experimental results.

V. CONCLUSIONS

We have obtained the dominant features of the wall-pressure field in a turbulent channel flow from a numerical solution to the Navier–Stokes equations with no closure assumptions. The root mean square pressure normalized on the wall shear stress is in excellent agreement with experiment. The smallest scales of the motion, however, could not be resolved, resulting in a slow broadband correlation decay rate. However, the asymptotic broadband convection speed is found to be in good agreement with experiment. Excellent agreement is found, up to a critical frequency, for the narrow-band phase speed. We anticipate that increased spatial resolution will improve the high-frequency results. The use of these numerical methods to determine the nature of the sources of the wall-pressure field appears to be feasible. More detailed results of the pressure field and the simultaneously computed velocity field will be given in a subsequent publication.

ACKNOWLEDGMENTS

The authors wish to thank Professor A. T. Patera for the development of the basic computer code used to make these studies and for useful discussions.

This work was supported by the Office of Naval Research under Contract No. N00014-83-K-0227 (MIT), Hydroacoustics Selected Research Opportunity (NRL), and the Naval Research Laboratory.

¹R. H. Kraichnan, *J. Acoust. Soc. Am.* **28**, 378 (1956).

²R. L. Panton and J. H. Linebarger, *J. Fluid Mech.* **65**, 261 (1974).

³M. T. Landahl, *J. Fluid Mech.* **29**, 441 (1967).

⁴S. A. Orszag and A. T. Patera, *Phys. Rev. Lett.* **47**, 832 (1981).

⁵P. Moin and J. Kim, *J. Fluid Mech.* **118**, 341 (1982).

⁶J. S. Bendat and A. G. Piersol, *Measurement and Analysis of Random Data* (Wiley, New York, 1966).

⁷W. K. Blake, *J. Fluid Mech.* **44**, 637 (1970).

⁸W. W. Willmarth and C. E. Woolridge, *J. Fluid Mech.* **14**, 187 (1962).

⁹H. H. Schloemer, *J. Acoust. Soc. Am.* **42**, 93 (1967).

¹⁰G. M. Corcos, *J. Fluid Mech.* **18**, 353 (1964).

¹¹J. M. Clinch, *J. Sound Vib.* **9**, 398 (1969).